

Vortex dynamics in a model left ventricle during filling

Bernardo Baccani^a, Federico Domenichini^{a,*}, Gianni Pedrizzetti^b

^a *Dipartimento Ingegneria Civile, Università di Firenze, V. S. Marta 3, 50139 Firenze, Italy*

^b *Dipartimento Ingegneria Civile, Università di Trieste, Piazzale Europa 1, 34127 Trieste, Italy*

Received 14 November 2001; received in revised form 17 June 2002; accepted 1 July 2002

Abstract

Analysis of the properties of the left ventricle flow during filling (diastole) is known to allow early detection of potential malfunctions during the fundamental heart pumping phase (systole). Diagnoses are now usually based on Doppler measurement of the flow velocity for which interpretative schemes and quantitative references are sought. The flow inside an ideal model of the left ventricle is here studied numerically by a finite difference method in prolate spheroid moving coordinates. The axisymmetric assumption is employed in this first study. The vortex dynamics is characterised by the formation of a wake vortex attached at the valvular edge which is shed at the end of the ventricle expansion. Major features are its translation by self-induced velocity and vortex-induced separations from the ventricle internal wall. Results are represented as, and compared with, clinical data showing a good general agreement and allowing an improved physical interpretation of the latter.

© 2002 Éditions scientifiques et médicales Elsevier SAS. All rights reserved.

Keywords: Vortex dynamics; Left ventricle; Diastole

1. Introduction

The development in medical disciplines has started to show, during last years, an increasing interest in quantitative and systematic approaches in support to the diagnostic and therapeutic activities. The objective stands in the possible early detection of pathologies and in the systematic refinement of therapeutic techniques. The fluid mechanics has contributed significantly in the last years to the modelling of the flow in large arterial vessels ([1–3], as recent examples, and references therein). A comparable accuracy of the numerical and experimental analysis has not yet been reached for the fluid dynamics of the heart. A cause for this delay may be found, among others, in the strong fluid–wall interaction which is fundamental in a cavity flow, like in the heart chambers, while it can be neglected, to a first approximation, in arterial flows [4]. The present work is focussed on the modelling of flow phenomena in a model of the left ventricle of the human heart.

The malfunction of the cardiac pump, in particular of the left ventricle, represents a primary cause of death in the modern society. Until few years ago the clinical studies were focussed to the pumping phase, i.e., the left ventricle contraction known as systole, whose pathologies represent a reduction in the heart's ability to pump the oxygenated blood in the circulation. It is now well known that a systolic pathology represents only the terminal stage of a generalised cardiac dysfunction whose initial minor symptoms can be recognised during the diastolic phase, i.e., the ventricle filling with the blood that enters from the left atrium through the mitral valve [5], therefore the early clinical diagnosis pays particular attention to the features of the diastolic filling. Diagnoses are commonly performed by mean of non-invasive techniques (magnetic resonance, echo-Doppler) which give an advanced but still incomplete picture of the fluid dynamics during the left ventricle filling, [6–8]: the typical diagnostic indicators have not a clear interpretation in terms of the corresponding mechanics and are thus difficult to be verified

* Correspondence and reprints.

E-mail address: federico@ingfi1.ing.unifi.it (F. Domenichini).

or quantified. An accurate modelling of the flow, and flow–wall interactions, inside the left ventricle is therefore necessary to improve the interpretation of the clinical observations on the basis of the physical phenomena.

The objective of the present work is to provide a further step in the numerical simulation of the fluid dynamics in an idealised model of the left ventricle during the unsteady filling period. Although the geometry employed is an oversimplification it represents an often used reference of the many possible realistic shapes, and results may eventually improve the understanding of the physical processes involved.

The study of the heart dynamics has initially developed by lumped, one-dimensional, models and slightly more complex schemes based on an inviscid fluid assumption; these have been able to capture the inertial effects and the pressure–volume relationship. The more realistic viscous flow assumption is necessary for the analysis of the vorticity-related dynamics, however the intensity and complexity of the vortex phenomena involved require a careful modelling. In fact, and just to give a preliminary picture of the dynamics, the impulsive inflow through the mitral valve is a severe localised vortex-jet, it enters with a velocity of the order of 1 m/s into a cavity of few centimetres length, it thus rapidly reaches the ventricle moving wall to interact with it and with the developing boundary layer.

Recently, numerical methods based on the finite elements or finite volumes schemes have been used to solve the fluid equations (CFD), in some cases coupled with models of the wall deformation. A first approach has been proposed [9] with finite three-dimensional volumes forced by a quasi stationary wall motion. In this scheme a realistic (dog) ventricular geometry has been prepared a priori, defining a set of configurations which change at given instants of time and are kept constant in between; the fluid equations are solved within these intervals of time imposing a flow through the wall during the integration. A method based on moving finite elements is applied to the systolic contraction, in the axisymmetric approximation [10,11], the coupled fluid–wall solution is obtained with an iterative scheme between two fluid and a solid dynamics packages. The strong flow–wall interaction is evidenced by the extremely small values of the relaxation constant for the convergence of the iterative method.

The diastolic phase has been analysed with an adaptive axisymmetric finite elements technique [12], with the wall finite displacements evaluated by a linear elastic membrane model with a time varying Young modulus, extending a one-dimensional scheme developed previously [13]. These adaptive finite elements are well suited for the solution of the motion characteristics as a whole, but require a significant computational effort to capture the local details of the flow field, particularly during the diastole. A high resolution is necessary to describe the thin vortex layer shed from the mitral valve, where the boundary-layer thickness is infinitesimal, and to solve the complex interaction between the incoming jet and the boundary-layer at the wall. A further difficulty is represented by the definition of the inlet velocity profile, depending on the scarcity of experimental data. An arbitrary choice of the velocity profile and a lack of resolution in some fundamental regions of the domain can lead to results significantly different from the actual dynamics. In [12] an initially ellipsoidal ventricle is assumed with the valve reproduced by extending the length beyond the maximum ellipsoid radius, also a smooth inlet profile is assumed; as a result the entering jet has a large front vortex which occupies the whole chamber, resembling the tube flow over an expansion [14]. Notwithstanding the points discussed above, and the possibly special choices introduced, that analysis currently represents the most accurate simulation of a model left ventricle under realistic conditions.

An alternative method for the coupled solution of the fluid–wall problem has been developed by introducing the concept of immersed boundary elements [15–18]: the fluid problem is solved on a regular domain (box), with a distribution of fictitious body forces. These replaces the presence of the wall, which in turn moves with the fluid within an iterative procedure, independently from the absolute, possibly unsteady, value of the fluid pressure being the boundary immersed in an incompressible fluid. It is well suited for reproducing the valve dynamics and has also a generality of application in arbitrarily complex three-dimensional geometry. On the other side this method suffers of a reduced accuracy in the boundary layers because the wall does not lie on coordinate curves and an interpolation is necessary. This method has been applied to the dynamics of the left heart [19,20] where the major features of the interaction are reproduced.

The left ventricle filling (diastole) has been reproduced in a laboratory experiment with the objective to get the same measurements as in clinics, under controlled conditions [21]. Such a model has been realised by a thin rubber ventricle communicating, through an orifice representing the mitral valve, to an above water tank at a given head level. The ventricle is immersed in a closed chamber with controlled pressure; the variation of pressure in the closed chamber drives the deformation of the rubber ventricle. During dilatation the flow enters through the mitral orifice to give a filling flow which remains essentially axisymmetric. The measured results are limited to a clinical-like M-mode, that is the space–time distribution of vertical component of velocity obtained by measuring it during time along the symmetry axis with a Doppler echograph.

The experimental results [21], as well as the numerical results [12], are in qualitative agreement between themselves and with clinical observation. On the basis of these a picture of the vortex dynamics occurring inside of the left ventricle can be given, at least for axisymmetric flows in normal (not pathologic) conditions. During the diastolic phase, the mitral jet generates a vortex ring which moves toward the ventricle apex, it interacts with the boundary-layer vorticity, and separation, when it approaches the ventricle wall. The details of the ventricle geometry are not significant during a large part of the diastolic phase until the jet gets closer to the walls, therefore, a prolate spheroid has been suggested by several authors as a geometry sufficiently representative of the actual configuration for the average of population [12], and references therein. More relevant parameters

are the geometry of the mitral valve, and the wall motion which also corresponds to the temporal law of the entering discharge; these can in fact be related to different pathologies of the valve or of the cardiac muscles.

In this work we consider an idealised model left ventricle under healthy conditions. It is modelled as a truncated prolate spheroid with the mitral valve, held open, corresponding to a thin circular orifice at the inlet. The flow is here assumed to be axisymmetric. These assumptions neglect the phenomena related to the three-dimensional geometry and to the valve movement at the beginning of the filling process; however this simple geometry is often used as a basic substitute for the many possible realistic shapes and is here adopted in order to define the reference phenomena, and to reduce the number of free parameters. Therefore, results should be read in a theoretical perspective as a basis for the more complex flow that may be encountered under realistic conditions. The system of equations written in primitive variables is solved numerically by a finite difference approach in boundary-fitted moving coordinates, allowing a next extension to three-dimensional flow. An accurate description of the vortex dynamics occurring in the idealised ventricle is presented, dependencies from the inlet orifice opening are systematically sought; comparisons with existing numerical and experimental findings are reported and interpretative schemes in terms of routine clinical observation are given. The mathematical problem is formulated in Section 2; the details of the numerical technique are reported in Section 3. Results are presented and discussed in Section 4; a conclusive discussion is reported in Section 5.

2. Mathematical formulation of the physical problem

2.1. Basic assumptions

We consider the flow inside a model left ventricle of an incompressible fluid with density ρ and kinematic viscosity ν . The ventricle is assumed to be half of a prolate spheroid with major semiaxis $H^*(t^*)$ and principal diameter $D^*(t^*)$, being t^* the time, and where $*$ denotes dimensional quantities. The mitral valve is modelled as an orifice of infinitesimal thickness in the equatorial plane, with a diameter $D_v^*(t^*)$; the ratio $m = D_v^*/D^*$ is kept constant in time. The system is forced by a given impulsive temporal law of the inlet flow-rate $Q^*(t^*)$ characterised by a rapid acceleration and a slower deceleration, with properties chosen on the basis of realistic primary (early) filling stage in healthy subjects. The inlet discharge also gives the ventricle volume variation; the dynamics of the two degrees of freedom ventricle geometry, $H^*(t^*)$ and $D^*(t^*)$, is described in Section 2.2 on the basis of a simple elastic wall modelling.

Given the axisymmetric ventricle geometry, the fluid flow is here assumed to be axisymmetric as well as. Although three-dimensional effects can be expected even in an axisymmetric geometry when the vortex dynamics grows in complexity, the present solution represents a first reference for the understanding of the basic phenomena and parameters involved.

The problem is made dimensionless assuming a reference time scale T and reference inlet velocity U , the reference unit of length is then $L = UT$, and the unit mass is taken as ρL^3 . The time scale T is chosen as the heartbeat period for convenience, therefore the early filling phase has a duration less than half unit time. A velocity scale, which is characteristic of the peak inlet velocity, is built from the available external data taking the peak inlet discharge and the area of the orifice at end systole ($t = 0$) when a valve diameter of $m = 0.8$ is chosen. The choices are suggested by the particular applied significance of this problem to have a formulation, i.e., $T \simeq 1$ s, $U \simeq 1$ m/s, that allows an easier readability of results and the immediate comparison with clinical data. In what follows dimensionless quantities are considered unless explicitly stated.

The mathematical system is given by the Navier–Stokes and continuity equations.

$$\frac{\partial \mathbf{v}}{\partial t} + (\mathbf{v} \cdot \nabla) \mathbf{v} = -\nabla p + \frac{1}{Re_T} \nabla^2 \mathbf{v}, \quad (1)$$

$$\nabla \cdot \mathbf{v} = 0, \quad (2)$$

where \mathbf{v} is the velocity vector, p the pressure, $Re_T = U^2 T / \nu$ is the Reynolds number corresponding to the chosen unit dimensions; a typical standard Reynolds number is $Re \sim Re_T D$. The boundary conditions at the walls, that the fluid velocity is equal to the wall velocity, gives the fluid–wall coupling; the conditions at the inlet represent a model for the upstream atrial flow.

The equations should be expressed in the moving, boundary-fitted, prolate spheroid system of coordinates $\{\mu, \eta\}$, which is related to the standard cylindrical coordinates $\{r, z\}$ by [22]

$$\begin{cases} r = \delta(t) \sinh(\alpha(t)\mu) \sin \eta, \\ z = \delta(t) \cosh(\alpha(t)\mu) \cos \eta. \end{cases} \quad (3)$$

The wall is thus described by two degrees of freedom dynamics: the functions $\delta(t)$ and $\alpha(t)$ are univocally related to the (positive) geometric properties by $\delta = (H^2 - D^2/4)^{1/2}$, $\alpha = \tanh^{-1}(D/2H)$. In these coordinates, the flow domain is

$\mu \in [0, 1] \times \eta \in [0, \pi/2]$ where the ventricle wall corresponds to the coordinate curve $\mu = 1$, the equatorial plane is $\eta = \pi/2$, and the axis of symmetry is along the two coordinate curves $\mu = 0$ and $\eta = 0$.

The characteristics of Eqs. (1), (2) expressed in the prolate spheroid coordinates, and the corresponding boundary conditions are reported in the following section. The dynamics of the wall motion and of the coordinate lines is introduced in Section 2.3.

2.2. Fluid dynamics

The vector form (1) of the Navier–Stokes equations is split in its scalar components, giving:

$$\begin{cases} \frac{\partial v_\mu}{\partial t} + \mathcal{C}_\mu(v_\mu, v_\eta, c_\mu, c_\eta, \delta, \alpha, \dot{\alpha}) + \mathcal{P}_\mu(p, \delta) - \frac{1}{Re_T} \mathcal{D}_\mu(v_\mu, v_\eta, \delta) = 0, \\ \frac{\partial v_\eta}{\partial t} + \mathcal{C}_\eta(v_\mu, v_\eta, c_\mu, c_\eta, \delta, \alpha, \dot{\alpha}) + \mathcal{P}_\eta(p, \delta) - \frac{1}{Re_T} \mathcal{D}_\eta(v_\mu, v_\eta, \delta) = 0; \end{cases} \quad (4)$$

where \mathcal{C} represents the convective terms, \mathcal{P} the pressure gradient, and \mathcal{D} the diffusive terms, and the condition of axial symmetry is already included. The quantities c_μ and c_η are the velocity of the coordinate system in the direction of coordinate curves; the mathematical expression of the different terms in (4) is reported in Appendix, with the main steps leading to them.

Eqs. (4) must be completed with the boundary conditions. The symmetry condition on the axis of the ventricle gives

$$v_\mu(0, \eta) = 0, \quad \left. \frac{\partial v_\eta}{\partial \mu} \right|_{0, \eta} = 0, \quad v_\eta(\mu, 0) = 0, \quad \left. \frac{\partial v_\mu}{\partial \eta} \right|_{\mu, 0} = 0. \quad (5)$$

The no-slip condition at the ventricle walls, $\mu = 1$, and on the closed part of the valvular plane, $\eta = \pi/2$ with $\mu \geq m$, reads

$$v_\mu = c_\mu, \quad v_\eta = c_\eta. \quad (6)$$

At the inlet section, $\eta = \pi/2$ and $\mu < m$, a profile of velocity must be imposed as to represent the properties of the incoming atrial flow. The flow inside the atrium accelerates to enter through the narrow mitral valve in the ventricle; the boundary layer is extremely thin because of the converging nature of the flow and of the extremely rapid unsteadiness parameters. In such a picture, given also the negligible mitral valve thickness, no finite boundary layer thickness can be estimated a priori. The inlet velocity profile is thus assumed to be irrotational; this conditions allows to evaluate the inlet profile at each instant during the numerical calculation, as specified in Section 3.

2.3. Wall dynamics

An exhaustive analysis of the fluid–wall interaction would be given by the coupled solution of the equations governing the fluid and wall dynamics [13,23,24]. A modelling of the latter requires the definition of the structural properties of the walls that, in the case of a ventricle, are those of a thick anisotropic shell with time-varying elastic properties (due to blood filling) in a non-linear finite deformation regime. In addition, the unsteady pressure profile in one place (at the inlet) must also be given. Models for the wall have been proposed for analysing the fluid–structure interaction [13,17,20].

The present work is focussed on the study of the flow properties and its dependence on the variability of the inlet condition; in this perspective, and since the structural parameters are not commonly measured, the fluid–wall coupled dynamics is not analysed rather the wall motion is assumed as given, because the flow phenomena do not change when the same wall motion is imposed or is computed by a coupled solution. Common clinical measurements concern the inlet mitral velocity [6], from which the temporal law of the entering discharge can be inferred, and, more roughly, the motion of the longitudinal and transversal lengths. These are used in the calculation to specify wall motion as described below.

A realistic time profile of the entering flow rate $Q(t)$ for an ideal early filling period can be represented as

$$Q = At^2 \exp(-ft), \quad (7)$$

where f is a deceleration frequency scale, and A is a scale for the total entering volume. Specification of the discharge law corresponds to give the time variation of volume $V = \frac{\pi}{6} D^2 H$ and gives a relation between the diameter and height derivatives

$$Q = \frac{\pi}{6} D^2 H \left(\frac{2}{D} \frac{dD}{dt} + \frac{1}{H} \frac{dH}{dt} \right). \quad (8)$$

An additional relation between the variations of diameter and height must be specified to close this two degrees of freedom problem.

We make the assumption that the relative dynamics can be inferred from a simplified relation derived from an elastic membrane model. The circumferential and meridional wall stresses in a prolate spheroid elastic membrane of vanishing thickness are, at the equatorial plane,

$$S_1 = \frac{pD}{4} \frac{8H^2 - D^2}{4H^2}, \quad S_2 = \frac{pD}{4}; \quad (9)$$

where p is the isotropic transmural pressure. Assume as a first approximation the linear elasticity relation $S_1 = E dD/D$, $S_2 = E dH/H$, where E is an instantaneous Young modulus, inserting these in (9) and eliminating p and E we obtain

$$\frac{dD}{D} = \frac{(8H^2 - D^2)}{4H^2} \frac{dH}{H}. \quad (10)$$

Relation (10) has the correct asymptotic behaviours that it must reduce to a sphere $dD/D = dH/H$ when $D = 2H$, and to the behaviour of a cylinder $dD/D = 2dH/H$ when $H \gg D$. It has been tested with one clinical data set and showed errors that could not be separated from the measurement uncertainty. Given the little available data and the possible large variation of real conditions, the approximation (10) represents a simplest first approach to model the wall dynamics on the basis of the only knowledge of an inlet flow-rate and an initial condition for the ventricle geometry. Inserting (10) into (8) we obtain an ordinary differential equation for the time evolution of the diameter

$$\frac{dD}{dt} = \frac{6Q}{\pi} \frac{8H^2 - D^2}{20H^3D - 2HD^3}, \quad (11)$$

and, from (10), of the ventricle height. Based on these the temporal evolution of prolate spheroid parameter δ and α defined in Section 2.1 can then be obtained.

3. Numerical method

The problem formulated in Section 2 has been numerically solved in primitive variables, with finite differences, using a fractional step method on a face-centred staggered grid [25,26]. In discretised form, the method can be summarised as follows: given a known velocity vector field \mathbf{u}^n and pressure field p^n at time step n , an intermediate non-solenoidal velocity $\hat{\mathbf{u}}$ is found by

$$\frac{\hat{u}_i - u_i^n}{\Delta t} = H_i^n - G_i(p^n) + \frac{1}{Re_T} D_i^n, \quad (12)$$

where H_i^n is the i th component of the non-linear term, G_i is the gradient operator here applied to pressure, D_i^n is the diffusive term. The solenoidal constrain is then forced by the correction

$$\frac{u_i^{n+1} - \hat{u}_i}{\Delta t} = -G_i(\phi^{n+1}), \quad (13)$$

where ϕ is a scalar potential which is evaluated at time step $n + 1$ by

$$\nabla^2 \phi^{n+1} = \frac{1}{\Delta t} \nabla \cdot \hat{\mathbf{u}}, \quad (14)$$

which is obtained taking the divergence of (13) and enforcing a solenoidal \mathbf{u}^{n+1} field. An estimate of the pressure field is eventually obtained

$$p^{n+1} = p^n + \phi^{n+1} + O\left(\frac{\Delta t}{Re_T}\right). \quad (15)$$

An explicit third-order Runge–Kutta scheme has been used for time advancement, the spatial derivative are approximated with a second-order finite differences scheme. The equations must be completed with the boundary-conditions. During the computation of the intermediate field $\hat{\mathbf{u}}$, the symmetry conditions (5) are imposed, and the no-slip conditions are enforced at the solid walls. The condition of zero-vorticity is used to specify the normal component of the velocity at the open inlet; in discrete form, such a condition becomes a linear relationship between the values of the tangential velocity, which are known at the points internal to the computational domain, and the values of the normal velocity, which are unknown at the grid points at the domain boundary. In such a way, a linear system of $N - 1$ equations can be written, being N the number of unknowns. The N -th linear equation corresponds to the numerical evaluation of the integral of the entering velocity, which must be equal

to the known value of the inlet discharge. The Poisson equation for the potential ϕ is completed by Neumann conditions at the symmetry axis and at the wall; a Dirichlet condition is forced at the inlet imposing a zero relative tangential velocity.

In order to obtain a better resolution close to the walls and in correspondence of the inlet edge, where large gradients are expected, stretched coordinates are adopted; in the η and μ directions

$$\eta_s = \frac{\pi \tanh(a_\eta \eta)}{2 \tanh(a_\eta)},$$

$$\mu_s = \left\{ 1 + b \sin[2\pi((c_1 + c_2 \mu_0)\mu + (c_3 + c_4 \mu_0)\mu^2)] \right\} \frac{\tanh(a_\mu \mu)}{\tanh(a_\mu)},$$

respectively, using constant grid sizes along the stretched variables. Several preliminary runs have been performed in order to define the proper grid resolution; the results reported in Section 4 have been obtained with grids 64×128 and 84×148 . The stretching parameter a_η ranges between 1.25 and 1.5; the coefficients $[c_1, c_3, c_3, c_4] = [-2, 4, -3, -4]$ are held fixed, the other parameters are chosen to ensure a sufficient resolution in correspondence of the sharp edge when m is varied with a_μ between 1.1 and 1.4, μ_0 in the interval $0.37 - 0.6$, $b \in [0.04, 0.14]$ with the exception of the case $m = 0.9$, where $b = 0$.

The time step has been chosen to guarantee the convective and diffusive stability conditions (namely a minimum value of $\Delta t = 2^{-14}$ is employed); the latter could not be ensured at the few points adjacent to the singular focus ($\mu = \eta = 0$) where the diffusive term only in (12) is however negligible being the flow there irrotational.

4. Results

4.1. Vortex dynamics phenomena

In what follows, the problem has been analysed fixing $Re_T = 2 \times 10^5$, which corresponds to a standard Reynolds number $Re \sim 2500$. The parameters A and f of Eq. (7) have been assumed equal to 0.385 and 20, respectively, these values can be taken as representative for subjects in healthy conditions. A detailed analysis of the flow evolution in the reference case $m = 0.7$ is first reported; the differences detected at different values of the valve closure are outlined afterward.

The flow evolution in term of vorticity dynamics is shown in Fig. 1, $m = 0.7$. The initial stage of motion is characterised by a rapid acceleration of the inlet flow; the flow field is almost irrotational, with the exception of the positive (counter clockwise) boundary-layer at the moving wall and of the thin vortex sheet separating at the inlet valvular sharp edge, Fig. 1(a) at $t = 0.0391$ (10/256). Immediately after its birth, the separating vortex-sheet rolls-up and forms a well defined vortex structure in an essentially self-similar inviscid dynamics as described in [27,28], having an internal size much smaller than the local external length scale which is the distance between the edge and the lateral wall. The presence of such a vortex induces the formation of a negative clockwise vorticity layer on the closed part of the mitral plane. During the following accelerating phase, the principal vortex is still attached to the edge, and grows in size and intensity; its influence on the wall vorticity dynamics can be observed in Fig. 1(b), $t = 0.082$ (21/256), where it induces a boundary-layer separation with secondary positive vorticity appearing at the wall. The decelerating phase, which starts at $t = 0.1$, leads to the truncation of the vortex sheet and the birth of a free vortex ring, Figs. 1(c) and 1(d), at $t = 0.1133$ (29/256) and 0.1367 (35/256), respectively. At the edge, a newly forming positive sheet guarantees the satisfaction of the Kutta condition. The subsequent evolution shows two different phenomena: at the inlet, the dynamics repeats with a less intense vortex, Figs. 1(e) at $t = 0.1758$ (45/256) and 1(f), $t = 0.2344$ (60/256); on the side wall the structure formed by the free ring induces a smooth separation and roll-up of the negative vorticity layer. The separated negative vorticity and the second positive vortex close to the inlet section can be observed in Fig. 1(g) at $t = 0.3516$ (90/256). During the final deceleration, the flow field shows a complex vorticity distribution with a mutual stretching and dissipation of the vortex structure that occupies a large part of the domain, Fig. 1(h), $t = 0.4492$ (115/256).

Enlarged views of the vorticity field close to the inlet edge are reported in Fig. 2 at three different instants of time, which correspond to those of Figs. 1(b), 1(c), and 1(d). The complex interaction between the attached sheet and the wall vorticity can be clearly appreciated in Fig. 2(a). At this time, the positive vortex has a size comparable with the length of the closed portion of the mitral plane, i.e., the local integral scale; the sharp growth of the induced secondary vorticity, particularly enhanced by the deceleration of the inlet flow, provokes the cut and detachment of the primary shed vortex, Fig. 2(b). The developing second positive vortex characterised by significant value of the vorticity is pushed toward the mitral wall, inducing there the formation of a negative layer, Fig. 2(c). A three layers vortex-structures is clearly observable at this time either on the side wall and on the mitral wall.

A further description of the flow evolution can be obtained from the velocity vectors, which are reported in Fig. 3 in conjunction with the pressure distribution. Given the arbitrary unsteady reference, the values of pressure relative to the value at (the centre of) the mitral plane are here given. At the initial stage of motion, the relative pressure field is dominated by the

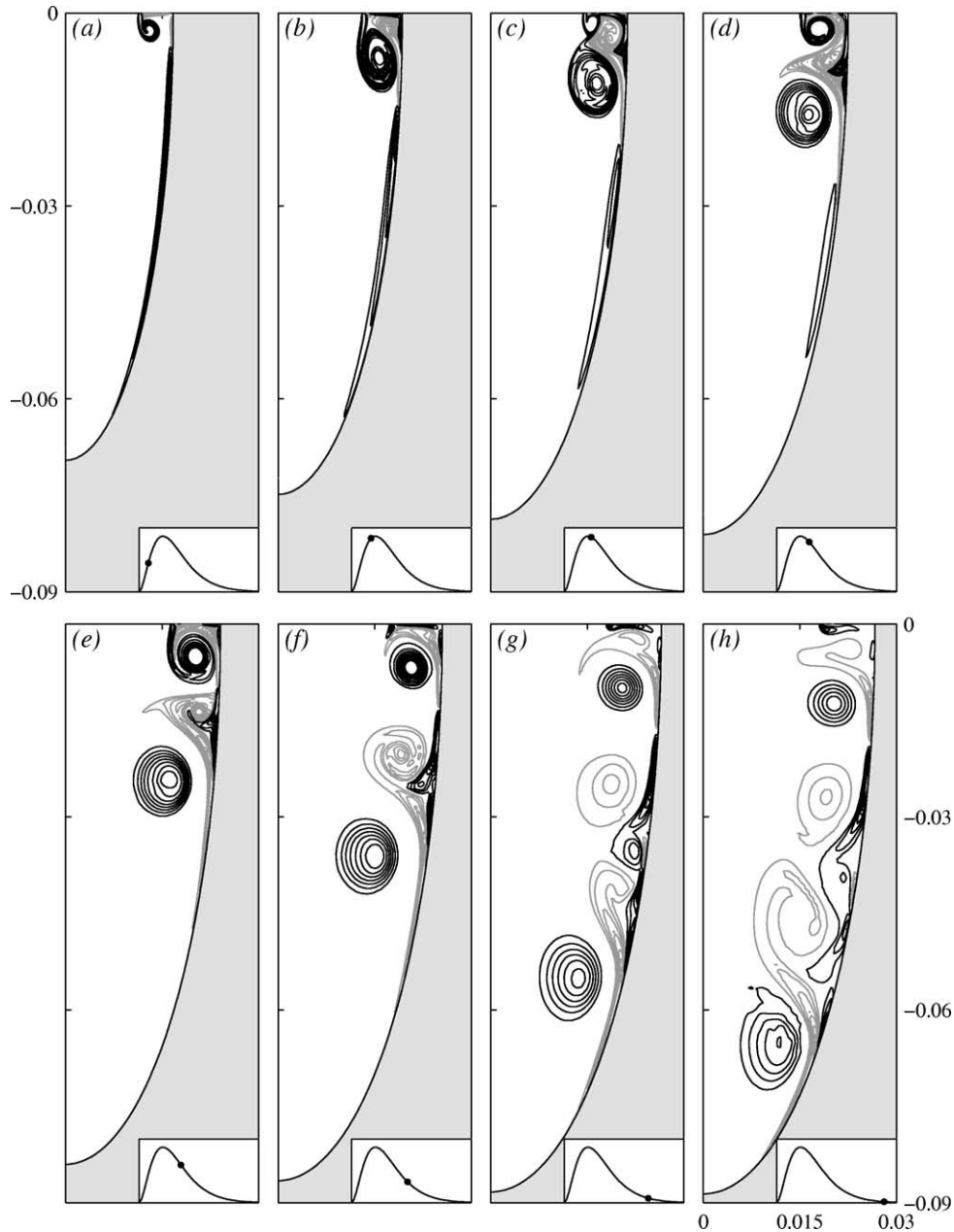


Fig. 1. Instantaneous vorticity fields, $m = 0.7$, $t = [1021\ 29\ 35\ 45\ 60\ 90\ 115]/256$. Positive levels (black) from 5 to 45, step 5; negative (grey) from -45 to -5 , step 5.

inertial contribution, it is negative inside the ventricle with a localised minimum in correspondence of the forming primary vortex. At the end of the accelerating phase the convective term becomes prevalent, giving positive values of the intraventricular pressure, Fig. 3(a) at $t = 0.082$ (21/256) to be compared with Fig. 1(b), especially in those places with smaller velocity. The primary detaching vortex and the second positive one forming at the edge are minima for centrifugal acceleration, while the local maximum between them is related to the accelerating characteristics of the flow field during the ejection phase, Fig. 3(b) at $t = 0.1367$ (35/256). Such a maximum tends to weaken, Fig. 3(c) at $t = 0.2344$ (60/256), and eventually to disappear once the process has terminated, Fig. 3(d) at $t = 0.4492$ (115/256). The final evolution shows the dominant contribution of the vortex structures, which progressively influences the large part of the flow domain. A similar evolution for either velocity and pressure has been described by Vierendeels et al. [12], where two positive vortex are detected during computation; however

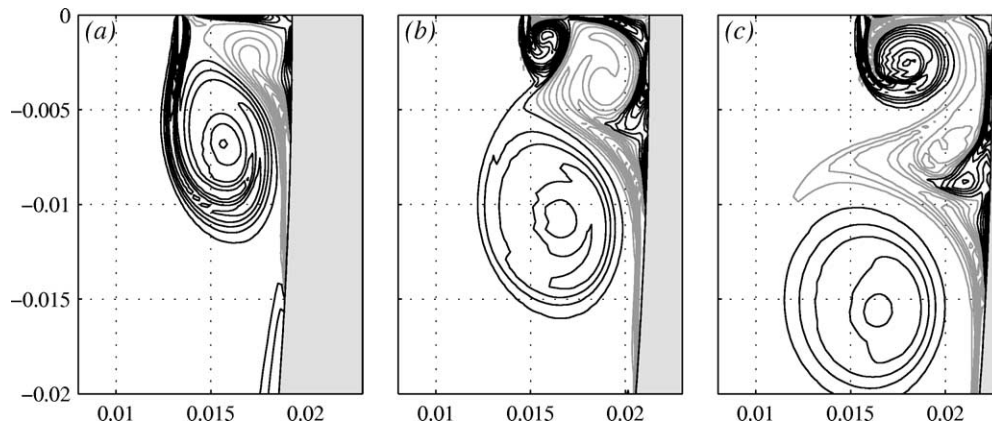


Fig. 2. Instantaneous vorticity fields, $m = 0.7$, $t = [21\ 29\ 35]/256$. Positive levels (black) from 5 to 105, step 10; negative (grey) from -105 to -5 , step 10.

those vortices are due to two consecutive filling waves, while in the present study a single flow pulse is considered during which the second vortex structure is formed. This difference is caused by the different assumption in the inlet flow where the blunt velocity profile assumed in [12] corresponds to a smoother vorticity distribution and dynamics.

The current inlet velocity is reported in Fig. 4 at times equal to those of Fig. 1. The initial profile, (a), corresponds to a field everywhere irrotational; at this time, the influence of the attached sheet is negligible; the progressive growth of the vorticity layer immediately downstream the edge leads to the smoothed profile (b). The subsequent deceleration with the truncation of the sheet modifies the local velocity distribution; the detaching portion becomes a further forcing term of the local balance of velocity, thus the Kutta condition is satisfied only by the still attached sheet, profiles (c) and (d). During the subsequent evolution the free vortex departs from the inlet section, the attached sheet develops, giving a more significant contribution to the local velocity, profiles (e) and (f). The final dynamics, profiles (g) and (h), is influenced by the detachment of the second positive vortex and by the presence of the negative one close to the edge. Such a presence provokes a local increment of the velocity, which is counterbalanced by the inversion of velocity at the centre of the orifice, such a phenomenon has been often observed during clinical Doppler measurements (G. Tonti, personal communication).

Similar analyses have been performed in correspondence of different values of the parameter m in the range 0.6–0.9, a comparison is reported in Fig. 5. The initial stage of the motion shows a similar dynamics, with a positive boundary-layer at the moving wall and a thin vortex sheet at the inlet edge. The intensity of the vorticity wake grows like the average inlet velocity, being here conserved the flow rate $Q(t)$ (ejection volume), when the area of the inlet orifice is decreased. The vorticity fields at $t = 0.1133$ (29/256), to be compared with Fig. 1(c), are plotted in Figs. 5 (a)–(c), for m equal to 0.6, 0.8, 0.9, respectively. The cases $m = 0.6$ and 0.8 appear very similar to the referring one previously discussed, while a less evident separation of the negative vorticity layer at the lateral wall is found at $m = 0.9$, Fig. 5(c). The subsequent dynamics appears much dependent on the mitral orifice opening. In the most narrow case, $m = 0.6$, the vortices detached from the mitral edge present a rapid motion, due to the superposition of the higher either external and self-induced velocities; moreover the increased distance from the lateral wall reduces the decelerating effect due to the wall itself (image effect). The final stage of the evolution shows a cavity almost completely filled by vortical flow, Fig. 5(d) at $t = 0.3516$ (90/256); an intense negative vortex close to the mitral wall deviates the inlet sheet toward the lateral wall. A completely different evolution has been detected in the case $m = 0.9$; the interaction between the vortex sheet and the lateral wall decelerates the motion of the first detached vortex and inhibits the birth of the second one, still present in the case $m = 0.8$, Figs. 5(e) and 5(f). When the valve is more open the vortices become weaker and move slower, they reach an increasingly limited deep inside the cavity; in the $m = 0.9$ case the shed vortex is seen to move backwards because its weakness reduces the self-induced velocity while the vicinity of the wall induces a negative image-induced velocity.

4.2. Major features

In the previous section, the vorticity dynamics has been analysed for various values of the geometric parameter m , showing quantitative differences of the initial dynamics, and a more evident dependence of the evolution on m during the decelerating phase. In order to define the principal features of the problem and to furnish useful interpretative schemes, the flow dynamics is here analysed in terms of representation more directly comparable with standard clinical observations.

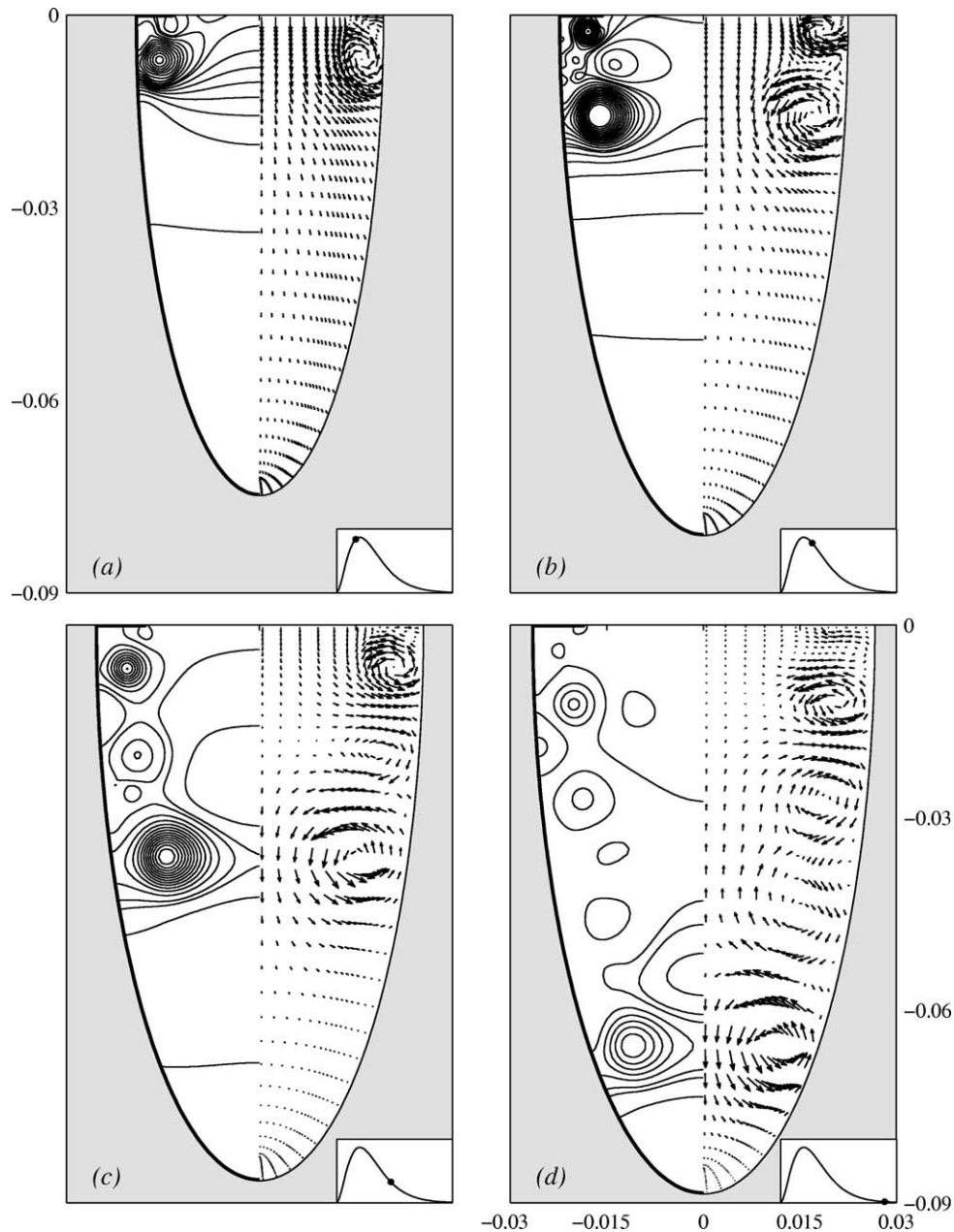


Fig. 3. Instantaneous velocity (right) and pressure fields (left), $m = 0.7$, $t = [21\ 35\ 60\ 115]/256$. Pressure levels: positive (black) from 0.01 to 0.53, step 0.04; negative (grey) from -0.53 to -0.01 , step 0.04.

In Fig. 6 the space–time map of the velocity on the symmetry axis is reported at $m = 0.7$ (the mitral plane is at $z = 0$), the vertical direction corresponds to space positions into the ventricle along its axis and the horizontal is the time. This representation corresponds to the common images obtained in clinics by Echocardiographic Color-Doppler M-mode to analyse the time development of ventricular filling [6]. During the initial acceleration, while the primary vortex is attached to the edge, the velocity increases at every point on the axis, with values ranging from the highest jet core, near the valvular plane, to the smaller velocity of the moving apex. Afterwards, as the vortex detaches and moves downstream at $t \simeq 0.12$, it creates an inclined band-like pattern of the velocity maxima on the axis. The slope of this trace corresponds to the propagation velocity of the vortex V_p , which is approximately constant during a first phase and decreases when the vortex approaches the ventricle apex. The value of this propagation velocity is often adopted as a pathological indicator of diastolic dysfunction [6].

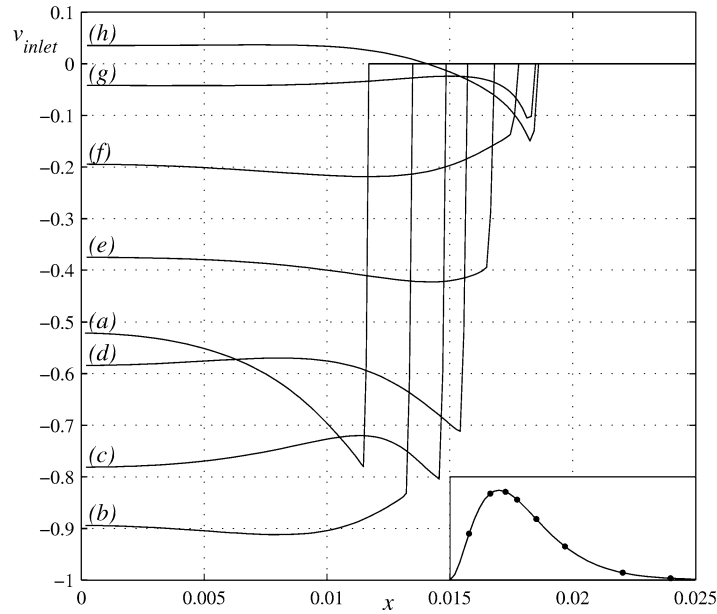


Fig. 4. Inlet velocity profiles, $m = 0.7$, $t = [10\ 21\ 29\ 35\ 45\ 60\ 90\ 115]/256$.

The axis velocity furnishes a limited description of the phenomena associated to the ventricular vortex dynamics; the space–time map of the vorticity at the ventricular lateral wall is reported in Fig. 7. Although this quantity is not easily measurable it gives an improved representation of the flow–wall interaction during ventricular filling. Initially the primary vortex generates a secondary, negative, vorticity wall layer, whose intensity is sufficient to induce a tertiary positive vorticity at the side wall, at $t \simeq 0.07$ and very close to the mitral plane, compare with Fig. 1(a). This wall vorticity structure moves downstream with the detached vortex, the zero-vorticity trace between them corresponds to the local maxima previously found in the axis velocity. The negative vorticity induced by the second vortex separated from the inlet edge is appreciable after $t \simeq 0.15$ in the upper portion of Fig. 7; the propagation velocity of the second vortex whose weakness prevents from being detectable in Fig. 6 is here recognised as much smaller than the primary one's.

The evolution of the axis pressure, relative to the mitral value, is given in Fig. 8. The initial negative intraventricular pressure is almost constant from the orifice to the apex (vertical contours), it is dominated by inertial effects, which are in phase with acceleration, until the development of the high velocity jet. The inversion of the spatial pressure gradient anticipates the maximum of the inlet flow rate, because the kinetic contribution, in phase with velocity itself, becomes dominant. A local reduction of pressure is found afterward in coincidence of the vortex sloping trace, which is clearly recognisable after $t \simeq 0.13$. An analogous behaviour has been noticed in the pressure distribution computed from clinical data of the axis velocity M-mode [7,8] with a quantitative agreement on the numerical values (notice that the current dimensionless pressure unit $\simeq 7.6$ mmHg).

Analogous results have been observed for the case $m = 0.6$, Fig. 9, where the more intense vortex separation gives a higher value of the propagation velocity V_p ; this can be detected either from the axis velocity and wall vorticity maps. In such a case, the influence of the second detached vortex becomes detectable also in the velocity evolution, upper portion of Fig. 9(a). The vorticity, Fig. 9(b), shows a sequel of alternating sign streaks, which represent the on-wall signature of the complex evolution reported in Fig. 5. The weakness of the separation process detected at $m = 0.9$ does not allow to recognise the propagation from the axis velocity space–time evolution, Fig. 10(a). The wall vorticity shows the trace of the vortex motion, which also presents a final weak backwards movement, Fig. 10(b). This negative propagation velocity is caused by the dominance of the vortex image due to the vicinity of the wall.

The M-mode representations can be directly compared with numerous common clinical observations. The two branches patter found here, the first vertical branch corresponding to the simultaneous entering jet and the second one to the vortex translation, is usually observed in vivo [6] and confirmed experimentally [21]. Sometimes the vortex branch is less visible depending from various possible parameters including, like here, geometrical ones. The quality of Echocardiographic data does not always allow to clearly recognise the patterns, and over estimations of the propagation velocity are often given when the slope of the first branch is assumed as the initial slope of the second one. A major qualitative difference with most in vivo data is the higher duration of the vortex found here, while its trace usually disappears in real M-mode well before it reaches the ventricle apex. This vortex persistence is a consequence of the axisymmetric approximation which neglects the three-dimensional vortex

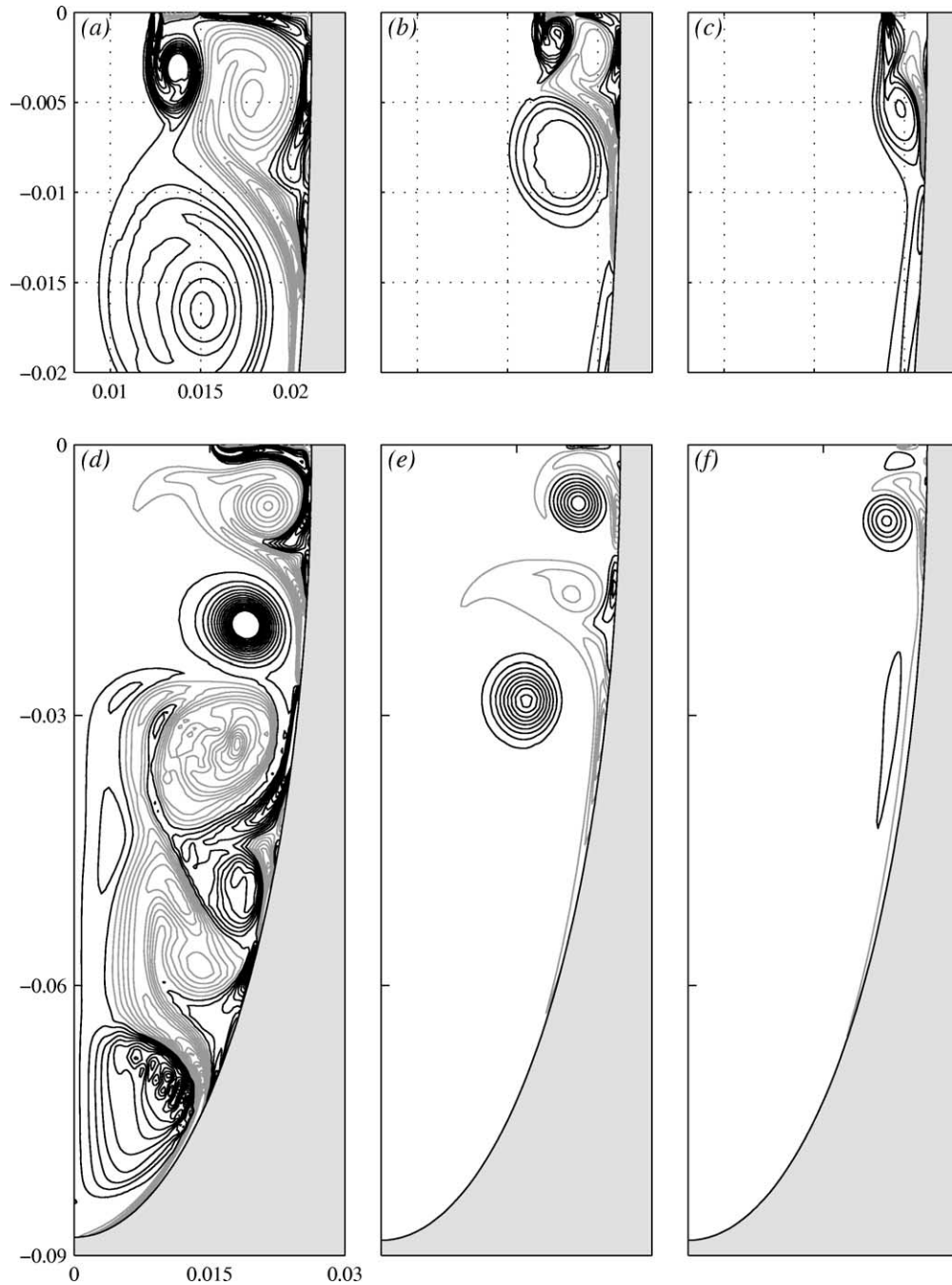


Fig. 5. Instantaneous vorticity fields at $t = 29/256$, (a) $m = 0.6$, (b) $m = 0.8$, (c) $m = 0.9$. Positive levels (black) from 5 to 105, step 10; negative (grey) from -105 to -5 , step 10. Instantaneous vorticity fields at $t = 90/256$, (d) $m = 0.6$, (e) $m = 0.8$, (f) $m = 0.9$. Positive levels (black) from 1.5 to 43.5, step 3; negative (grey) from -43.5 to -1.5 , step 3.

instabilities and related dissipative phenomena. The presence of wake vortex during the filling phase has been recognised in careful MRI (Magnetic Resonance Imaging) clinical measurements [29]. A non-symmetric nature of the wake vortex has also been recognised from MRI [30], thus suggesting the need for a three-dimensional modelling to capture the evolution of the wake after the formation phase.

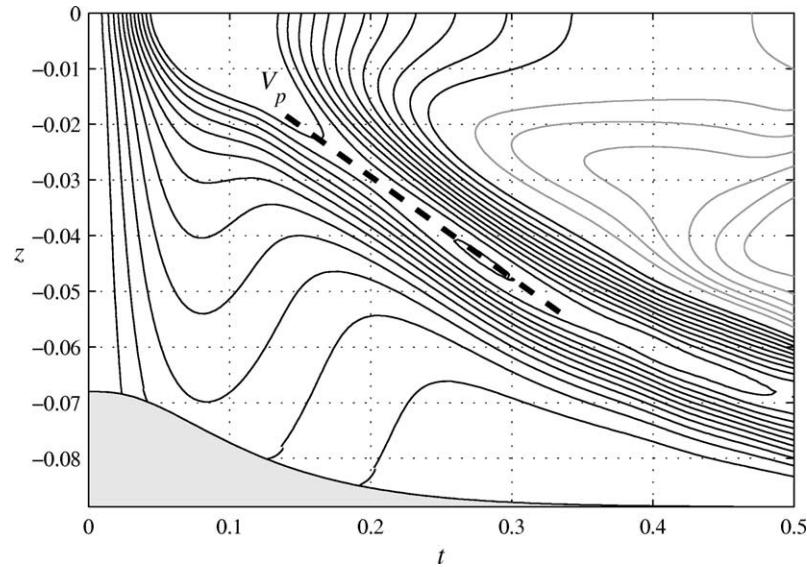


Fig. 6. Space–time map of the axis velocity, $m = 0.7$. Positive levels (grey) from 0.05 to 0.6, step 0.05; negative (black), from -0.6 to -0.05 , step 0.05.

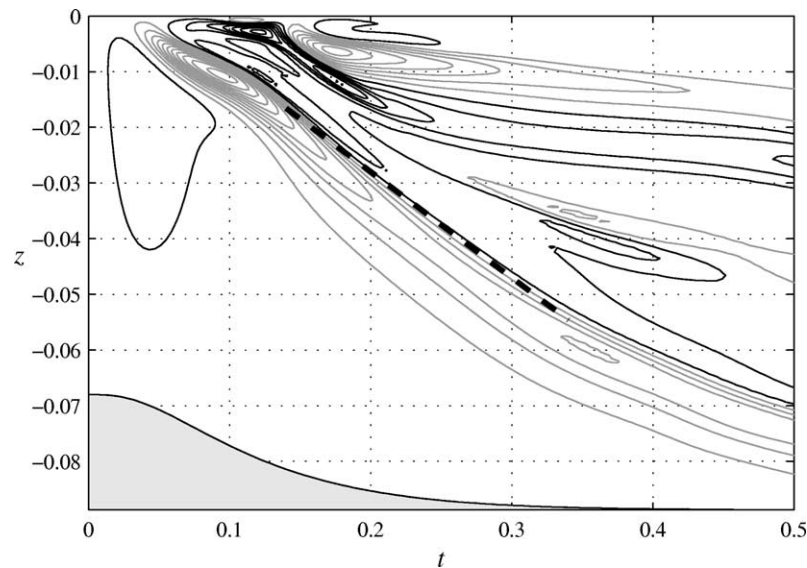


Fig. 7. Space–time map of the side wall vorticity, $m = 0.7$. Positive levels (black) from 20 to 680, step 40; negative (grey), from -680 to -20 , step 40.

The time evolution of the pressure difference between the apex and the mitral plane is plotted in Fig. 11, for the four valvular openings. In all cases the pressure drop shows a minimum at the maximum acceleration of the entry flow, reported above in the same figure, and a maximum pressure gain in correspondence of the maximum inflow. The pressure profile is in good agreement with the results in [12] despite the differences in the vortex pattern, confirming that integral pressure differences are not much dependent on the flow details. Therefore inertial contribution, in phase with the flow acceleration, dominates the very initial period, then convective effects increase until they become preponderant (pressure in phase with inflow) at maximum flow in agreement with clinical observations [7,8]. During the subsequent deceleration, the pressure difference decays to zero, with local influences of the vorticity structures particularly evident in the $m = 0.6$ case.

The propagation velocity is a quantity commonly adopted in the clinical practice as an indicator of specific pathologies. It corresponds to the vortex celerity, and gives a measurable estimate of its strength, although other effects influence the value. In

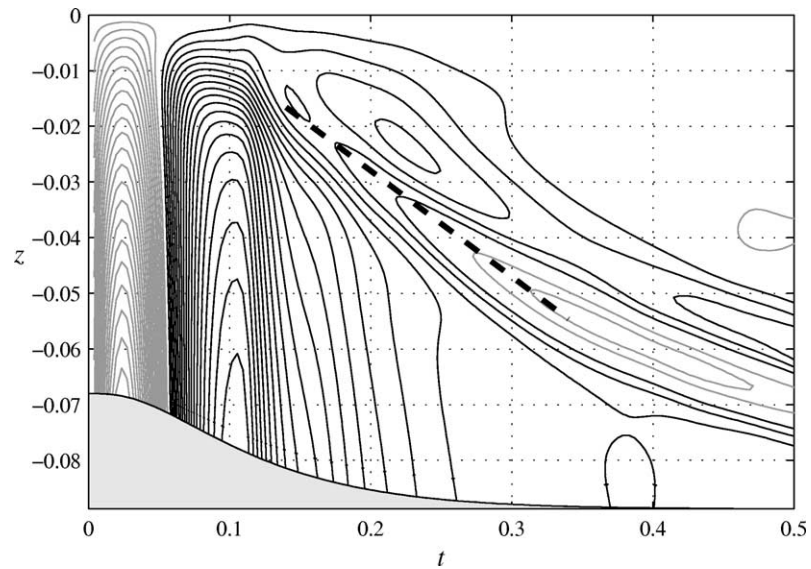


Fig. 8. Space-time map of the relative axis pressure, $m = 0.7$. Positive levels (black) from 0.02 to 0.5, step 0.02; negative (grey) from -0.5 to -0.02 , step 0.02.

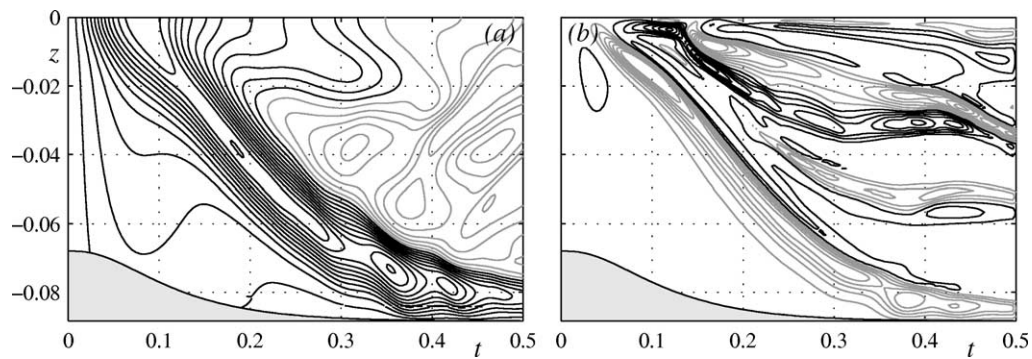


Fig. 9. Space-time map of the axis velocity (a), $m = 0.6$, positive levels (grey) from 0.05 to 1.15, step 0.1, negative (black) from -1.15 to -0.05 , step 0.1. Space-time map of the side wall vorticity (b), positive levels (black) from 30 to 410, step 60, negative (grey) from -410 to -30 , step 60.

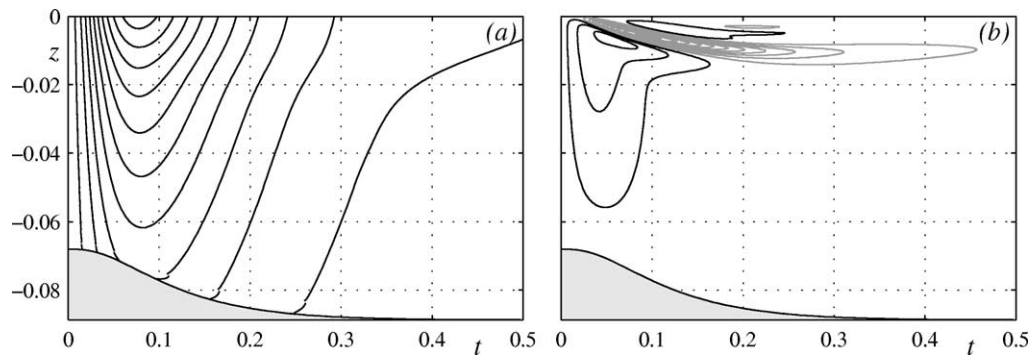


Fig. 10. Space-time map of the axis velocity (a), $m = 0.9$, positive levels (grey) from 0.025 to 0.6, step 0.05, negative (black) from -0.6 to -0.025 , step 0.05. Space-time map of the side wall vorticity (b), positive levels (black) from 10 to 210, step 20, negative (grey) from -210 to -10 , step 20.

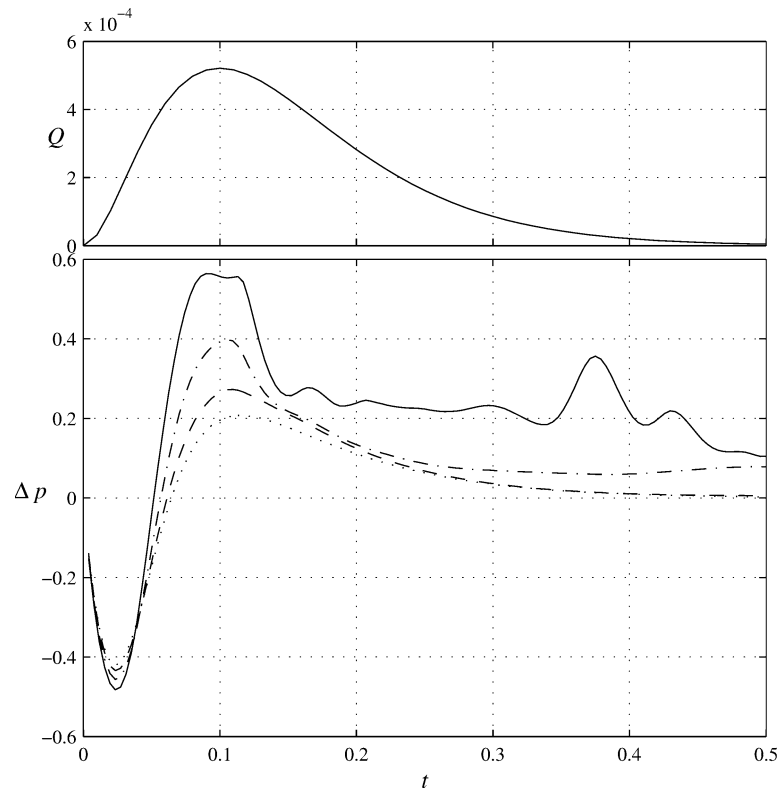


Fig. 11. Time evolution of the pressure difference between the apex and the mitral plane; solid line $m = 0.6$, dash-dotted line $m = 0.7$, dashed line $m = 0.8$, dotted line $m = 0.9$.

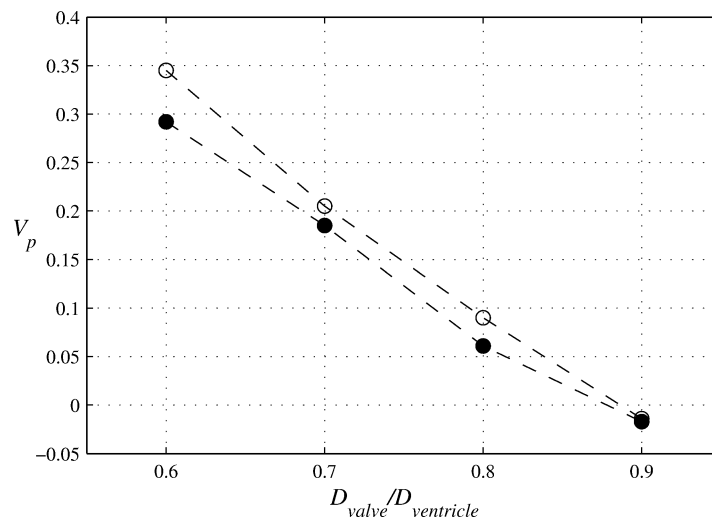


Fig. 12. Propagation velocity V_p of the primary vortex; (●) flow rate (7), (○) modified flow rate.

the present idealised case the vortex velocity is expected to decrease with the opening of the valve. This is evidenced in Fig. 12, where the estimated V_p values are reported. Filled circles correspond to the flow rate (7), the same quantity is plotted with open circles as given by a different inlet discharge

$$Q = 0.0037 t^{1/2} \exp(-(10t)^{1.1}),$$

which has the same total inlet volume and peak value of (7), with a more rapid accelerated phase. This gives a stronger wake and consequent higher values of V_p .

5. Conclusions

The diastolic flow inside of a model left ventricle in healthy conditions has been studied by numerical solution of the equations of motion with a boundary-fitted moving coordinates system in a prolate spheroid geometry. The problem is assumed to be forced by a given variation of the ventricle volume with a temporal law chosen on the basis of clinical data for the early filling phase; a simplified scheme for the relative dynamics of the wall degrees of freedom has been introduced. The flow has been analysed at different values of the mitral valve diameter, here modelled as an orifice of infinitesimal thickness.

The solution has been described in terms of vorticity dynamics, which has shown common features in all the analysed cases. The initial phase is characterised by the birth and development of a vortex sheet attached to the inlet valvular edge which immediately rolls-up to form a compact vortex. This induces a vorticity layer of opposite sign at the lateral wall of the ventricle, which eventually separates. The primary vorticity detaches from the valvular sharp edge when the inlet flow decelerates, and forms a vortex ring that moves downstream toward the ventricle apex. This motion is accompanied by the translation along the lateral wall of the vortex-induced double-layer vorticity structure. The intensity of the primary separated vortex and its propagation velocity are influenced by the degree of closure of the mitral valve with more intense vortices in correspondence of narrower valves.

The vorticity dynamics has been analysed in relation with the spatial and temporal evolution of quantities usually measured in the clinical practice, such as the axis velocity and pressure. The comparative analysis has shown the direct dependence of the velocity and pressure behaviour on the dynamics of the primary detached vortex; the propagation velocity represents the signature of the vortex motion inside of the ventricle cavity, it is commonly estimated by echocardiography and adopted as an indicator of specific pathologies. The dependence of propagation velocity with valve closure is evaluated, it is a measure of the wake strength and decreases with increasing valve diameter. In those cases characterised by a weak separation process, the axis velocity and pressure are not able to show any ventricular vortex dynamics which on the opposite is clearly recognisable in the evolution of the wall vorticity. Intraventricular pressure is dominated by inertia during the early acceleration and by convection afterward in presence of the high inlet velocity.

The results here reported represent a preliminary, theoretical, part of a study aimed to support the physical interpretation of phenomena observed clinically, and to complete the physiological picture obtained by the available diagnostic instrument. Results are in agreement with a previous axisymmetric simulation of a similar system [12] despite the several differences in the modelling that was there more focussed on the fluid–wall interaction. Results are in qualitative agreement with clinical *in vivo* data (Echographic and MRI), the main differences can be imputable to neglecting non-axisymmetric dissipation.

The system is here approximated as an axisymmetric flow in an axisymmetric geometry thus neglecting the eventual role of three-dimensional dynamics; the fixed valve hypothesis also neglects the leaflets influence during their opening. These assumption prevents from drawing conclusions to be applied to the many different conditions in which real hearts operate, they have been employed to define the basic vortex phenomena involved in a well controlled system with a minimal number of free parameters. Additional features that would introduce further complexity should be included progressively. A three-dimensional numerical modelling of the flow is now in progress by introducing non-zero spectral modes in the same geometry; such an approach will allow to reproduce the whole heartbeat period by including the lateral, aortic, outflow. More realistic three-dimensional elastic geometry, that may account for internal ventricular features, should then be analysed on the basis of specific medical data and suggestions.

Acknowledgements

The authors are indebted to Gianni Tonti MD for the enthusiastic cardiological supervision and suggestions. The authors acknowledge financial support from the University of Trieste and from Italian MURST.

Appendix

We start from the Navier–Stokes equations in axisymmetric cylindrical coordinates $\{r, z\}$. In order to properly derive the influence of the time-varying coefficients $\delta(t)$ and $\alpha(t)$ in the time derivative we proceed by a two steps transformation.

We first introduce moving cylindrical coordinates $\{\tilde{r}, \tilde{z}\} = \delta^{-1}\{r, z\}$ and we write the equations in these scaled cylindrical coordinates.

$$\begin{cases} \frac{\partial u_z}{\partial t} + \frac{\partial u_z}{\partial \tilde{r}} \left(\frac{u_r}{\delta} - \tilde{r} \frac{\dot{\delta}}{\delta} \right) + \frac{\partial u_z}{\partial \tilde{z}} \left(\frac{u_z}{\delta} - \tilde{z} \frac{\dot{\delta}}{\delta} \right) = -\frac{1}{\delta} \frac{\partial p}{\partial \tilde{z}} + \frac{1}{\delta^2 Re_T} \left[\frac{\partial^2 u_z}{\partial \tilde{z}^2} + \frac{\partial^2 u_z}{\partial \tilde{r}^2} + \frac{1}{\tilde{r}} \frac{\partial u_z}{\partial \tilde{r}} \right], \\ \frac{\partial u_r}{\partial t} + \frac{\partial u_r}{\partial \tilde{r}} \left(\frac{u_r}{\delta} - \tilde{r} \frac{\dot{\delta}}{\delta} \right) + \frac{\partial u_r}{\partial \tilde{z}} \left(\frac{u_z}{\delta} - \tilde{z} \frac{\dot{\delta}}{\delta} \right) = -\frac{1}{\delta} \frac{\partial p}{\partial \tilde{r}} + \frac{1}{\delta^2 Re_T} \left[\frac{\partial^2 u_r}{\partial \tilde{z}^2} + \frac{\partial^2 u_r}{\partial \tilde{r}^2} + \frac{1}{\tilde{r}} \frac{\partial u_r}{\partial \tilde{r}} - \frac{u_r}{\tilde{r}^2} \right], \end{cases} \quad (A1)$$

where $\dot{\delta}$ denotes time derivative.

Eqs. (A1) are written in a corresponding preliminary prolate spheroid coordinates $\{\tilde{\mu}, \eta\}$, which are related to $\{\tilde{r}, \tilde{z}\}$ by $\tilde{z} = \cosh(\tilde{\mu}) \cos \eta$, and $\tilde{r} = \sinh(\tilde{\mu}) \sin \eta$, by standard coordinate transformation. Afterward a further transformation of coordinates is performed to introduce the time varying coefficient $\alpha(t)$, writing the final pair $\{\mu, \eta\} = \{\alpha^{-1} \tilde{\mu}, \eta\}$.

The resulting convective and diffusive operators in Eqs. (4) are finally

$$\begin{aligned} C_\mu &= \frac{1}{h_\mu} \frac{\partial v_\mu}{\partial \mu} (v_\mu - c_\mu) + \frac{1}{h_\eta} \frac{\partial v_\mu}{\partial \eta} (v_\eta - c_\eta) + \frac{v_\eta}{\alpha h_\eta^2} \frac{\partial h_\mu}{\partial \eta} \left(v_\mu - c_\mu + \mu h_\mu \frac{\dot{\alpha}}{\alpha} \right) - \frac{v_\eta}{h_\mu h_\eta} \frac{\partial h_\eta}{\partial \mu} (v_\eta - c_\eta), \\ C_\eta &= \frac{1}{h_\mu} \frac{\partial v_\eta}{\partial \mu} (v_\mu - c_\mu) + \frac{1}{h_\eta} \frac{\partial v_\eta}{\partial \eta} (v_\eta - c_\eta) - \frac{v_\mu}{h_\mu h_\eta} \frac{\partial h_\mu}{\partial \eta} \left(v_\mu - c_\mu + \mu h_\mu \frac{\dot{\alpha}}{\alpha} \right) + \frac{v_\mu}{h_\mu^2} \frac{\partial h_\mu}{\partial \mu} (v_\eta - c_\eta); \end{aligned} \quad (A2)$$

$$\begin{aligned} D_\mu &= \frac{1}{h_\mu^2} \frac{\partial^2 v_\mu}{\partial \mu^2} + \frac{1}{h_\eta^2} \frac{\partial^2 v_\mu}{\partial \eta^2} + \frac{1}{h_\mu^2 h_\eta} \frac{\partial v_\mu}{\partial \mu} \frac{\partial h_\theta}{\partial \mu} + \frac{2}{h_\mu^2 h_\eta} \frac{\partial v_\eta}{\partial \mu} \frac{\partial h_\mu}{\partial \eta} + \frac{1}{h_\eta^2 h_\theta} \frac{\partial v_\mu}{\partial \eta} \frac{\partial h_\theta}{\partial \eta} \\ &\quad - \frac{2}{h_\mu h_\eta^2} \frac{\partial v_\eta}{\partial \eta} \frac{\partial h_\eta}{\partial \mu} - \frac{v_\mu}{h_\mu} \left[\frac{1}{h_\eta^2} \frac{\partial^2 h_\mu}{\partial \eta^2} + \frac{1}{h_\mu^2} \frac{\partial^2 h_\mu}{\partial \mu^2} + \frac{1}{h_\mu} \left(\frac{\partial h_\theta}{\partial \mu} h_\theta \right)^2 \right] - \frac{2v_\eta}{h_\mu^2 h_\eta h_\theta} \frac{\partial h_\mu}{\partial \mu} \frac{\partial h_\theta}{\partial \eta}, \end{aligned} \quad (A3')$$

$$\begin{aligned} D_\eta &= \frac{1}{h_\mu^2} \frac{\partial^2 v_\eta}{\partial \mu^2} + \frac{1}{h_\eta^2} \frac{\partial^2 v_\eta}{\partial \eta^2} + \frac{2}{h_\mu h_\eta^2} \frac{\partial v_\mu}{\partial \eta} \frac{\partial h_\eta}{\partial \mu} - \frac{2}{h_\mu^2 h_\eta} \frac{\partial v_\mu}{\partial \mu} \frac{\partial h_\mu}{\partial \eta} + \frac{1}{h_\mu^2 h_\theta} \frac{\partial v_\eta}{\partial \mu} \frac{\partial h_\theta}{\partial \mu} \\ &\quad + \frac{1}{h_\eta^2 h_\theta} \frac{\partial v_\eta}{\partial \eta} \frac{\partial h_\theta}{\partial \eta} - \frac{v_\eta}{h_\eta} \left[\frac{1}{h_\eta^2} \frac{\partial^2 h_\eta}{\partial \eta^2} + \frac{1}{h_\mu^2} \frac{\partial^2 h_\eta}{\partial \mu^2} + \frac{1}{h_\eta h_\theta^2} \frac{\partial h_\theta}{\partial \eta} \right] - \frac{2v_\mu}{h_\mu h_\eta^2 h_\theta} \frac{\partial h_\theta}{\partial \mu} \frac{\partial h_\eta}{\partial \eta}, \end{aligned} \quad (A3'')$$

while the gradient operator for pressure is $\mathcal{G}_i = (1/h_i) \partial / \partial x_i$.

The c_μ, c_η functions are the velocity components of the moving grid in physical space

$$c_\mu = \dot{\delta} \delta \frac{\sinh(\alpha\mu) \cosh(\alpha\mu)}{h_\eta} + \mu h_\mu \frac{\dot{\alpha}}{\alpha}, \quad c_\eta = -\frac{\dot{\delta} \delta \sin \eta \cos \eta}{h_\eta};$$

where the metric coefficients of coordinates defined in (3) are [22]

$$[h_\mu, h_\eta, h_\theta] = \delta \left[\alpha \sqrt{\cosh^2(\alpha\mu) - \cos^2 \eta}, \sqrt{\cosh^2(\alpha\mu) - \cos^2 \eta}, \sinh(\alpha\mu) \sin \eta \right].$$

References

- [1] R. Botnar, G. Rappitsch, M.B. Scheidegger, D. Liepsch, K. Perktold, P. Boesiger, Hemodynamics in the carotid artery bifurcation: a comparison between numerical simulations and in vitro MRI measurements, *J. Biomech.* 33 (2000) 137–144.
- [2] S.Z. Zhao, X.Y. Xu, A.D. Hughes, S.A. Thom, A.V. Stanton, B. Ariff, Q. Long, Blood flow and vessel mechanics in a physiologically realistic model of a human carotid bifurcation, *J. Biomech.* 33 (2000) 975–984.
- [3] M. Grigioni, G. Pedrizzetti, A. Amodeo, C. Daniele, C. D'Avenio, L. Zovatto, R.M. Di Donato, A comparison between numerical and PIV studies of the flow through a total cavopulmonary connection, *Int. J. Artif. Organs* 23 (8) (2000) 579.
- [4] G. Pedrizzetti, F. Domenichini, A. Tortoriello, L. Zovatto, Pulsatile flow inside moderately elastic arteries, its modelling and effects of elasticity, *Comput. Methods Biomech. Biomedical Engng.* 5 (3) (2002) 219–231.
- [5] L. Mandinov, F.R. Eberli, C. Seiler, O.M. Hess, Review: Diastolic heart failure, *Cardiovas. Res.* 45 (2000) 813–825.
- [6] M.J. Garcia, J.D. Thomas, A.L. Klein, New Doppler echocardiographic applications for the study of diastolic function, *J. Am. Coll. Cardiol.* 32 (1998) 865–875.
- [7] M.S. Firstenberg, P.M. Vandervoort, N.L. Greenberg, N.G. Smedira, P.M. McCarthy, M.J. Garcia, J.D. Thomas, Noninvasive estimation of transmitral pressure drop across the normal mitral valve in humans: importance of convective and inertial forces during left ventricular filling, *J. Am. Coll. Cardiol.* 36 (6) (2000) 1942–1949.

- [8] G. Tonti, G. Pedrizzetti, P. Trambaiolo, A. Salustri, Space and time dependency of inertial and convective contribution to the transmitral pressure drop during ventricular filling, *J. Am. Coll. Card.* 38 (1) (2001) 290–291.
- [9] T.W. Taylor, T. Yamaguchi, Realistic three-dimensional left ventricular ejection determined from computational fluid dynamics, *Med. Eng. Phys.* 17 (8) (1995) 602–608.
- [10] A. Redaelli, F.M. Montevecchi, Computational evaluation of intraventricular pressure gradients based on a fluid–structure approach, *J. Biomech. Eng.* 118 (1996) 529–537.
- [11] A. Redaelli, F.M. Montevecchi, Ventricular mechanics during the ejection phase, in: P. Verdonck, K. Perktold (Eds.), in: *Intra and Extracorporeal Cardiovascular Fluid Dynamics*, Vol. 2, WIT Press, Southampton, 2000, pp. 129–175.
- [12] J.A. Vierendeels, K. Riemsdagh, E. Dick, P.R. Verdonck, Computer simulation of intraventricular flow and pressure during diastole, *J. Biomech. Eng.* 122 (2000) 667–674.
- [13] J. Vierendeels, P. Verdonck, E. Dick, Intraventricular pressure gradient and the role of pressure wave propagation, *J. Cardiovas. Diagnosis and Procedures* 14 (3) (1997) 147–152.
- [14] G. Pedrizzetti, Unsteady tube flow over an expansion, *J. Fluid Mech.* 310 (1996) 89–111.
- [15] C.S. Peskin, D.M. McQueen, A three-dimensional computational method for blood flow in the heart: I Immersed elastic fibers in an incompressible fluid, *J. Comput. Phys.* 81 (1989) 372–405.
- [16] C.S. Peskin, D.M. McQueen, A three-dimensional computational method for blood flow in the heart: II Contractile fibers, *J. Comput. Phys.* 82 (1989) 289–298.
- [17] C.S. Peskin, B.F. Printz, Improved volume conservation for the three-dimensional Navier–Stokes equations involving an immersed moving membrane, *J. Comput. Phys.* 105 (1993) 33–46.
- [18] D.M. McQueen, C.S. Peskin, Shared-memory parallel vector implementation of the immersed boundary method for the computation of blood flow in the beating mammalian heart, *J. Supercomputing* 11 (3) (1997) 213–236.
- [19] J.D. Lemmon, A.P. Yoganathan, Three-dimensional computational model of left heart diastolic function with fluid–structure interaction, *J. Biomech. Eng.* 122 (2000) 109–117.
- [20] D.M. McQueen, C.S. Peskin, A three-dimensional computer model of the human heart for studying cardiac fluid dynamics, *Computer Graphics* 34 (2000) 56–60.
- [21] T. Steen, S. Steen, Filling of a model left ventricle studied by colour M mode Doppler, *Cardiovas. Res.* 28 (1994) 1821–1827.
- [22] P.M. Morse, H. Feshbach, *Methods of Theoretical Physics*, McGraw-Hill, New York, 1953.
- [23] X.Y. Luo, T.J. Pedley, A numerical simulation of unsteady flow in a two-dimensional collapsible channel, *J. Fluid Mech.* 314 (1996) 191–225.
- [24] G. Pedrizzetti, Fluid flow in a tube with an elastic membrane insertion, *J. Fluid Mech.* 375 (1998) 39–64.
- [25] J. Kim, P. Moin, Application of a fractional-step method to incompressible Navier–Stokes equations, *J. Comput. Phys.* 59 (1985) 308–323.
- [26] R. Verzicco, P. Orlandi, A finite-difference scheme for three-dimensional incompressible flow in cylindrical coordinates, *J. Comput. Phys.* 123 (1996) 402–414.
- [27] D.I. Pullin, The large-scale structure of unsteady self-similar rolled-up vortex sheets, *J. Fluid Mech.* 88 (1978) 401–430.
- [28] B. De Bernardinis, J.M.R. Graham, K.H. Parker, Oscillatory flow around disks and through orifices, *J. Fluid Mech.* 102 (1981) 279–299.
- [29] W.Y. Kim, P.G. Walker, E.M. Pedersen, J.K. Poulsen, S. Oyre, K. Houliand, A.P. Yoganathan, Left ventricular blood flow patterns in normal subjects: a quantitative analysis by three-dimensional magnetic resonance velocity mapping, *J. Am. Coll. Cardiol.* 26 (1995) 224–238.
- [30] P.J. Kilner, G.Z. Yang, A.J. Wilkes, R.H. Mohiaddin, D.N. Firmin, M.H. Yacoub, Asymmetric redirection of flow through the heart, *Nature* 404 (2000) 759–761.